Influence of the polymer architecture and functionalization with carboxylate groups over the release of octenidine hydrochloride from poly(lactic acid)-based nanoparticles

Matteo Maraldi[1], Anna Guida[1], Mattia Sponchioni[1,], and Davide Moscatelli[1]*

[1] Department of Chemistry, Materials and Chemical Engineering "Giulio Natta", Politecnico di Milano, Via Luigi Mancinelli 7, 20131 Milano, Italy.

** Corresponding author: Mattia Sponchioni, Email: mattia.sponchioni@polimi.it*

Abstract

Health care associated infections affect every year more than four million people due to the increasing resistance of bacteria to traditional antibiotics. In turn, the systematic use of quaternary ammonium salts as antiseptics is hampered by their inherent toxicity and high hydrophilicity that leads to their rapid elimination from the body. Therefore, a carefully controlled release of these antiseptics is pivotal to achieve prolonged therapeutic efficacy reducing the side effects. In this work, high encapsulation efficiencies and good control over the release of octenidine hydrochloride from poly(lactic acid) (PLA)-based nanoparticles (NPs) was achieved by introducing functional carboxylate groups in the polymer. The influence of the polymer structure and functionalization over the drug release was sistematically investigated. Star-like and brush-like polymers with tunable number of ionizable chain end-groups were synthesized *via* combination of ring-opening polymerization and reversible addition−fragmentation chain transfer polymerization. These polymers were formulated in NPs and loaded with octenidine through emulsion/solvent evaporation. Brush-like polymers demonstrated to be a versatile tool for the modulation of the initial burst and long term release of the antiseptic through the tuning of the electrostatic interactions between the negative groups on the polymer, whose number can be precisely controlled, and the positively charged drug.

Keywords: Polylactic acid; Octenidine hydrochloride; Polymer nanoparticles; Drug delivery; Ionizable polymers

1 Introduction

Biodegradable polymeric nanoparticles (NPs) are attracting increasing interest in many fields of medicine and biology[1–3]. In fact, this type of colloids shows promise in applications ranging from the controlled release of therapeutics to imaging and diagnosis[4–7]. Regarding drug delivery, polymer NPs have been widely studied as carriers for lipophilic drugs, enabling their systemic administration[8–10]. With this strategy, the bioavailability of the drugs in aqueous environments is improved and toxic species or solvents necessary for their formulation are avoided. In addition, the

degradability of the polymers in physiological conditions, coupled with the biocompatibility and the easiness of excretion of the degradation products, prevents their accumulation in the body[2,11–13]. In the literature, polyester-based NPs are the golden standard[14–16]. These showed promising results in the controlled release of lipophilic therapeutics. On the other hand, the encapsulation and controlled release of charged drugs, which are more prone to solubilize in water, is more difficult due to the poor affinity between the drug and the hydrophobic polymer[17]. At the same time, manifold drugs fall into this category and a carrier for their sustained release is therefore urgently required.

Among these drugs, it is worth citing antibiotics and antiseptics, which are generally positively charged at physiological conditions. The research on these therapeutics is becoming crucial in the last years in order to face the issue of health care associated infections (HCAIs). In fact, HCAIs are one of the most urgent problems to be solved in healthcare and more specifically in intensive care units[18–20]. The prevention and treatment of this type of nosocomial infections are hampered by two factors. First, the increasing number of multiply resistant bacterial strain resulting from an accelerated microbial evolution due to the massive abuse of antibiotics by the society in the past years[21]. Indeed, as an example, *Staphylococcus aureus* showed first the resistance against methicillin in the 50s and then against vancomycin later in the 90s[22,23], whereas nowadays we are experiencing a wide spreading of *Staphylococcus epidermidis*, which is resistant to riphampicin[24]. Second, the short lasting action of the therapeutics currently used allows the organization of pathogens in *biofilms*. These are structures which are able to significantly enhance their capacity to resist to antibiotics[25]. This is even more likely to occur on surfaces as tubes, catheters and implantable devices, normally present in the hospitals. For these reasons, the treatment of HCAIs is shifting from antibiotics towards well tolerated antiseptics and in particular to quaternary ammonium salts (QAS)[26]. Among these, octenidine hydrochloride (OHC) proved to be a promising molecule against these pathologies[27,28]. OHC is a quaternary ammonium compound characterized by an efficient antimicrobial activity against a broader spectrum of bacteria than the widely diffuse chlorhexedine. It is active against both gram positive and gram negative bacteria, even when biofilms are present, and it is already commercialized for topical use[28–31]. Unfortunately, the possibility of adopting OHC to treat *in vivo* infections is hampered by its inherent toxicity and rapid excretion through biological fluids and renal filtration, which limits its therapeutic index[32]. These considerations force a carefully controlled release of this drug, to avoid side effects to healthy tissues and maximize its therapeutic efficacy[32]. To face these problems, drug delivery systems able to gradually release OHC during time have been developed. Remarkable examples are NPs composed by mesoporous silica[33], wound dressings made up of nanocellulose and combinations of nanocellulose with amphiphilic copolymers containing OHC[34,35], and poly(glycolyc acid) (PGA)-based biodegradable suture[36]. The microencapsulation of OHC in polymeric devices is highly beneficial for the possibility of keeping the drug concentration during time in the range between the minimum inhibitory concentration (MIC), thus ensuring its antiseptic activity, and the cytotoxicity threshold[37]. Then, the adoption of biodegradable polymer NPs introduce the additional advantage of a systemic administration of the drug and the prevention of side effects in healthy tissues. Nonetheless, the difficulty in controlling precisely the encapsulation and release of positively charged drugs like OHC represents a major obstacle towards the clinical application[38].

A possible strategy to enhance the encapsulation efficiency and improve the drug retention inside polymer NPs relies on the electrostatic interaction between the positive drug and negative functional groups in the polymer chains[39]. In this work, the influence of ionizable carboxylate groups added

to the polymeric chains and of the polymer architecture over the encapsulation and sustained release of OHC from biodegradable NPs was systemically investigated. Specifically, poly(lactic acid) was synthesized in two different architectures, namely star-shaped and brush-like. Star-shaped polymers were synthesized *via* ring opening polymerization (ROP) of D,L-lactide from pentaerythritol as initiator. On the other hand, for the brush-like architectures, two oligo(lactic acid) macromonomers with different chain lengths were synthesized *via* ROP using 2-hydroxyethylmethacrylate (HEMA) as initator. These biodegradable macromonomers were further polymerized *via* reversible addition−fragmentation chain transfer (RAFT) polymerization to achieve good control over the molecular weight distribution and the number of units added to the polymer chains[40]. Since the oligo(lactic acid) macromonomers can be easily provided with an ionizable carboxylate end-group *via* succyniclation, the RAFT polymerization enabled also to precisely control the number of charged groups per polymer chain. From these polymers we produced NPs loaded with OHC in a single emulsification and solvent evaporation step, which allowed to decouple the molecular weight of the polymer from the particle size. Given the similar size of all of the NPs, we showed that there is a linear correlation between the number of carboxylic groups per particle and the capacity of retaining the drug by the formulation. Furthermore, the number of ionizable groups deeply influences the kinetic constant of the first-order model that reproduces the experimental stustained release. Thus, the modulation of the number of ionizable groups per particle is an appealing strategy for controlling the encapsulation and release rate of OHC, enabling to maintain its concentration within a desired therapeutic window.

2 Materials and Methods

2.1 Materials

3,6-Dimethyl-1,4-dioxane-2,5-dione (LA, 98%, MW = 144.13 g/mol), Toluene (99.7%, MW = 92.14 g/mol), 2-Hydroxyethyl methacrylate (HEMA, 97%, MW = 130.14 g/mol), tin(II) 2-ethylhexanoate ($Sn(Oct)_2$, 92.5-100%, MW = 405.12 g/mol), sodium sulfate (Na_2SO_4, ≥ 99%, MW = 142.04 g/mol), succinic anhydride (99%, MW = 100.07 g/mol), 4-(Dimethylamino)pyridine (DMAP, ≥ 99.9%, MW = 122.17 g/mol), dichloromethane (DCM, ≥ 99%, MW = 84.93 g/mol), hydrochloric acid 0.1M (Stabilized, MW = 36.46 g/mol), 4,4'-Azobis(4-cyanovaleric acid) (ACVA, ≥ 98%, MW = 280.28 g/mol), 4-Cyano-4-(phenylcarbonothioylthio)pentanoic acid (CPA, ≥ 97%, MW = 279.38 g/mol), ethanol (≥ 99.8%, MW = 46.07 g/mol), 1,4-Dioxane anhydrous (≥ 99.8%, MW = 88.11 g/mol), diethyl ether (DEE, ≥ 99.8%, MW = 74.12 g/mol), N-Hydroxysuccinimide (NHS, ≥ 98%, MW = 115.09 g/mol), N,N′-Dicyclohexylcarbodiimide (DCC, ≥ 99.8%, MW = 206.33 g/mol), Methanol (MeOH, ≥ 99.8% MW = 32.04 g/mol), 1,8-diazabyciclo[5.4.0]-undec-7-ene (DBU, ≥ 99% MW = 152.24 g/mol), 2,2-Bis(hydroxymethyl)-1,3-propanediol (pentaerythritol, ≥ 99%, MW = 136.15 g/mol), benzoic acid (≥ 99.5% MW = 122.12 g/mol), dimethyl sulfoxide (DMSO, ≤ 0.02% water, MW = 78.13 g/mol), TWEEN® 80 (viscous liquid, MW = 1310 g/mol), deuterochloroform (Cl_3OD, 99.8%, MW = 120.38 g/mol), tetrahydrofuran (THF containing 250 ppm BHT as inhibitor, anhydrous, ≥ 99.9%, MW = 72.11 g/mol) were purchased from Sigma-Aldrich, Germany and used as received unless specifically noted. Octenidine hydrochloride (OHC) was purchrased from Schülke

& Mayr GmbH, Germany. All the chemicals and the solvents used were of analytical-grade purity. Dichloromethane and dimethyl sulfoxide were dried using molecular sieves (3Å).
Lactide was first recrystallized in order to remove all the impurities and different isomers present in the commercial product. Therefore, LA was dissolved in toluene at 90°C at 200 g/L. Then, the obtained solution was stored overnight at T = -20 °C thus allowing the crystallization of lactide. Successively, the lactide crystals were recovered from the solvent through filtration and dried in a vacuum oven at 40 °C for 48 h.

2.2 Synthesis of oligo(lactic acid) macromonomers

Two biodegradable macromonomers, hereinafter $HEMALA_n$, being *n* the average degree of polymerization of lactic acid, were synthetized *via* ROP of the recrystallized LA in bulk, using HEMA as initiator and $Sn(Oct)_2$ as catalyst. The $Sn(Oct)_2$ to HEMA molar ratio was set to 1/200 and Na_2SO_4 was added to remove traces of water present in the reaction mixture. The ratio between the monomer and initiator was set to the desired average degree of polymerization (*n*). In particular, two different macromonomers with *n* equal to 4 and 8 were produced, namely $HEMALA_4$ and $HEMALA_8$. As an example, for $HEMALA_8$, 10.19 g of LA, 102 mg of Na_2SO_4, 2.3 g of HEMA and 36 mg of $Sn(Oct)_2$ were added to a round bottom flask equipped with a magnetic stirrer and a rubber cap and were heated in a constant temperature oil bath to 110 °C. The polymerization was carried out at 110 °C for 4 hours, under stirring. At the end of the reaction, an aliquot of 10 mg of the obtained macromonomer was dissolved in 0.7 mL of deuterated chloroform, in order to measure the conversion (χ) and *n* via ^{1}H-NMR (performed on a Bruker 400 MHz spectrometer), according to **Equations S1** and **S2**. Furthermore, an aliquot of 8 mg was dissolved in 2 mL of THF and filtered with a 0.2 μm polytetrafluoroethylene (PTFE) filter, with the aim of analysing the molecular weight distribution *via* gel permeation chromatography (GPC, Jasco *2000* Series). The separation was performed using THF as eluent, at a flow rate of 1 mL/min and a temperature of 35 °C. The instrument was equipped with three styrene/divinyl benzene (SDV) columns (Polymer Standards Service, Germany; pore size 10^3, 10^5 and 10^6 Å; 300 mm length and 8 mm internal diameter), a precolumn (50 mm length and 8 mm internal diameter) and a differential refractive index (RI) detector. The calibration curve was constructed with poly(styrene) (PS) standards (from 580 to 3'250'000Da).
An aliquot of the produced macromonomers was then functionalyzed with a –COOH end-group by succinylation with succinic anhydride, using DMAP as catalyst and DCM as solvent. Succinic anhydride was added with a 50% molar excess compared to $HEMALA_n$ and a DMAP to succinic anhydride molar ratio equal to 0.2 was set. In the case of $HEMALA_{8\text{-}COOH}$, 3.6 g of $HEMALA_8$ and 0.76 g of succinic anhydride were dissolved in 18 mL of anhydrous DCM (13% w/w) in a round bottom flask with a magnetic stirrer and a rubber cap. Then 0.19 g of DMAP were dissolved in 4 mL of anhydrous DCM in a vial and poured in the flask. The mixture was left to react with stirring at room temperature. After 24 hours, the obtained solution was washed with 20 mL of HCl 0.1 M. Then, Na_2SO_4 in large excess was added to the organic phase containing DCM and polymer in order to remove water; the solution was then filtered with a filter paper to remove the salt. Finally, the organic solvent was evaporated under reduced pressure. An aliquot of the final product was analysed via ^{1}H-NMR in deuterated chloroform and the reaction conversion (χ) was calculated according to **Equation S3**.

2.3 RAFT agent functionalization

The carboxylic acid group of the CPA was capped with a O-methyl ester through a two steps procedure: (i) the CPA was reacted with NHS, (ii) the obtained product was reacted with MeOH in DCM. Specifically, 1 g of CPA and 0.45 g of NHS were dissolved in 30 mL of anhydrous DCM in a 100 mL round bottom flask equipped with a magnetic stirrer. The flask was sealed with a rubber cap and wrapped in a tinfoil paper. Then, 0.96 grams of DCC dissolved in 20 mL of anhydrous DCM were added and the mixture was incubated at 25 °C under magnetic stirring for 24 hours. The final solution was filtered to remove dicyclohexylurea. The product was then washed four times with 40 mL of distilled water in a 500 mL separating funnel. Na_2SO_4 in large excess was added to the organic phase containing DCM and CPA-NHS to remove water. The solution was filtered with a filter paper to remove the salt and the solvent evaporated under reduced pressure. Hence, 200 mg of the obtained product were dissolved in 5 mL of MeOH and 7 mL of DCM in a 25 mL round bottom flask equipped with a rubber cap and a magnetic stirrer. The mixture was heated to 25 °C under magnetic stirring for 24 hours. Then, the product was dried under reduced pressure in order to remove the unreacted MeOH and purified by recrystallization from a 4:1 v/v ethyl acetate/hexane mixture at 60 °C. The pink crystals of CPA-MeOH were recovered with a yield of 75%. An aliquot of the product was analysed via ^{1}H-NMR in deuterated chloroform. The reaction conversion (χ) was evaluated according to **Equation S6**.

2.4 Synthesis of brush-like polymers

PLA brush-like polymers with two target number-average molecular weights (Mn), 20 kg/mol and 50 kg/mol, were synthesized *via* RAFT polymerization of the macromonomers previously produced *via* ROP, with and without the carboxy functionalization. In addition, polymers with the same target molecular weight were produced using the CPA-MeOH and $HEMALA_4$ obtained *via* ROP, without -COOH functionalization, in order to synthesize carboxy-free brush-like polymers of 20 kg/mol and 50 kg/mol. The initiator to RAFT agent molar ratio was set to 1/3 in all of the synthesis. The degree of polymerization (*p*) for each mancromonomer was set as the molar ratio between the macromonomer itself and the RAFT agent leading to the desired Mn. As an example, to synthetize 28-$HEMALA_8$, being 28 the target degree of polymeryzation *p* required to reach Mn = 20 kg/mol, 1 g of $HEMALA_8$, 5 mg of ACVA and 14 mg of CPA were dissolved in 10 mL of ethanol and 1.2 mL of 1,4-dioxane in a round bottom flask equipped with a magnetic stirrer and a rubber cap. The solution was purged by bubbling nitrogen for 15 minutes and heated to 65 °C in an oil bath under stirring for 24 hours. Then, the obtained polymer was precipitated in a 10-fold excess of diethyl ether and an aliquot of the recovered product was analysed *via* ^{1}H-NMR in deuterated chloroform, in order to evaluate the monomer conversion (χ) and the degree of polymerization (*p*), according to **Equations S4** and **S5**. The final polymers were also analyzed *via* GPC as previously explained, in order to evaluate Mn and dispersity (Đ).

2.5 Synthesis of the star-shaped polymers

The synthesis of a star-shaped PLA was performed *via* ROP using pentaerythritol as initiator and DBU as catalyst. The degree of polymerization per single arm was set as the molar ratio between the

moles of LA and the moles of hydroxyl groups from the initiator. The DBU to pentaerythritol molar ratio was set to 0.8. Na_2SO_4 was added to the reaction to keep anhydrous the system and benzoic acid was used to quench the reaction. Benzoic acid to DBU molar ratio was set to 1.2.
Thus, in order to achieve star-shaped polymers with a targeted molecular wight of 20 kg/mol, 5.14 g of recrystallized lactide were dissolved with 51 mg of Na_2SO_4 and 70 mg of pentaerythritol in 11 mL of anhydrous DMSO in a round bottom flask equipped with a magnetic stirrer and sealed with a rubber cap. The solution was purged by bubbling nitrogen for 15 minutes at room temperature. Hence, a solution of 67 mg of DBU in 2 mL of anhydrous DMSO was fed to the round bottom flask dropwise and the reaction was performed at room temperature under stirring. After 4 hours, a solution of 0.6 g of benzoic acid in 4 mL of anhydrous DMSO was added to quench the reaction and deactivate the catalyst. The purification of the polymer was performed *via* dialysis for three days against 1 L of absolute ethanol using a selective permeable SpectraPor regenerated cellulose membrane (molecular weight cut-off = 3.5 kDa). Then, an aliquot of the obtained product was analyzed *via* ^{1}H-NMR in deuterated chloroform and GPC. The monomer conversion (χ) and degree of polymerization (p) were calculated from ^{1}H-NMR spectra in accordance with **Equations S7 and S8**, while Mn and Đ were measured *via* GPC.
Then, some of the star-shaped polymers synthesized were functionalized through the addition of succinic anhydride, using DMAP as catalyst, to provide the polymer with the carboxy functionalization. Succinic anhydride was added in 50% molar excess and the DMAP to succinic anhydride molar ratio was set to 0.2.
Briefly, 1.3 g of star-shaped polymer and 56 mg of succinic anhydride were dissolved in 6.54 mL of anhydrous DCM (13% w/w) in a round bottom flask with a magnetic stirrer and a rubber cap. Hence, a solution obtained mixing 13 mg of DMAP in 1 mL of DCM was added to the round bottom flask and the mixture was left to react with stirring at room temperature for 24 hours.
Afterwards, the obtained solution was washed with 15 mL of HCl 0.1 M. Later, Na_2SO_4 in large excess was added to the organic phase containing DCM and the polymer in order to remove the remaining water. The solution was then filtered with a filter paper. The organic solvent was finally evaporated under reduced pressure.
An aliquot of the final dried product was analysed *via* ^{1}H-NMR in deuterated chloroform and the monomer conversion (χ) was calculated according to **Equation S9**.

2.6 Synthesis of polymeric NPs loading OHC

Drug-loaded PLA-based NPs were synthetized *via* sonication/emulsion and solvent evaporation process, using the brush-like and star-shaped PLA. Briefly, 100 mg of the selected polymer and 12 mg of OHC were dissolved in 2.4 mL of DCM and poured in a vial. Then, 7.6 mL of water solution containing 10 mg of TWEEN 80 were added. The system was emulsified for 30 seconds with a probe sonicator (UP200S, Hielscher Ultrasound Technology), maintaining the amplitude to 50%. Finally, the DCM was evaporated under reduced pressure to form the final NPs. The NP size (*Dn*), polydispersity (PdI) and ζ-potential were evaluated *via* dynamic light scattering (DLS) with a Zetasizer Nano ZS (Malvern, Instruments) at a scattering angle of 173°. All the NP suspensions were diluted to 0.5% w/w in deionized water before the DLS measurements. Three measurements were performed for each sample and the results reported are relative to the average of the three measurements.
Scanning electron Microscopy (SEM) was performed on NPs of two different polymers architectures, *i.e.* a brush-like and a star-shaped polymer. The SEM micrographs were carried out on a Zeiss EVO 50 XVP microscope with an electron high tension (EHT) of 10.00 kV.

2.7 Drug encapsulation efficiency and release tests

In order to evaluate the drug encapsulation, after the synthesis, an aliquot of the NP suspension was added to a 20 mL Vivaspin (Sartorius, molecular weight cut-off = 10 kDa, polyethersulfone membrane) and centrifugated for 30 minutes at 5000 rpm. The solution of water containing the released OHC filtrated completely into the lower part of the Vivaspin, while the polymer NPs remained inside the upper part of the membrane. An aliquot of the water solution containing OHC was diluted 10 times and then analysed *via* UV-Vis spectroscopy (Jasco V-630 UV Spectrophotometer) measuring the absorbance at 280 nm. The intensities of the signals were related to OHC concentration in water through a calibration curve, according to **Figure S7**. The encapsulation efficiency was finally calculated according to **Equation 1**, defining C_0 the initial OHC concentration and C the measured octenidine concentration.

$$Encapsulation\ \% = \frac{C_0 - C}{C_0} * 100 \quad (1)$$

Whereas, in order to investigate the kinetic of release of the drug, the NP suspension was inserted in a permeable SpectraPor membrane (molecular weight cut-off = 6-8 kDa) and placed in a beaker containing 200 mL of distilled water under mild stirring. The top of the beaker was covered to avoid evaporation of water. The amount of OHC released at different timepoints was evaluated by measuring the absorbance at 280 nm of the aqueous buffer using the protocol previously described and according to **Equation 2**.

$$Drug\ released\ \% = \frac{C}{C_{max}} * 100 \quad (2)$$

where C is the drug concentration in water measured at different times and C_{max} the maximum concentration of Octenidine achievable, considering the complete release of the drug.
After two weeks, the NP size (*Dn*), polydispersity (PdI), and ζ-potential were evaluated via DLS.

3 Results and Discussion

3.1 NP synthesis

First, we synthesized biodegradable, PLA-based polymers with two different architectures, namely brush and star-shaped, *via* combination of ROP and RAFT polymerization, as shown in **Figure 1a-b**.
Specifically, brush-like polymers were produced through a two step process. In the first reaction, two oligo(lactic acid) macromonomers were synthesized *via* ROP. The living nature of the ROP allowed us to define *a priori* the average degree of polymerization (*n*) of each macromonomer by modulating

the mole ratio between the monomer and the initiator (n = 4, 8)[41]. As shown in **Table 1**, we produced macromonomers with low dispersity (Đ) and n close to the target (see **Figure S1** for ^{1}H-NMR characterization).

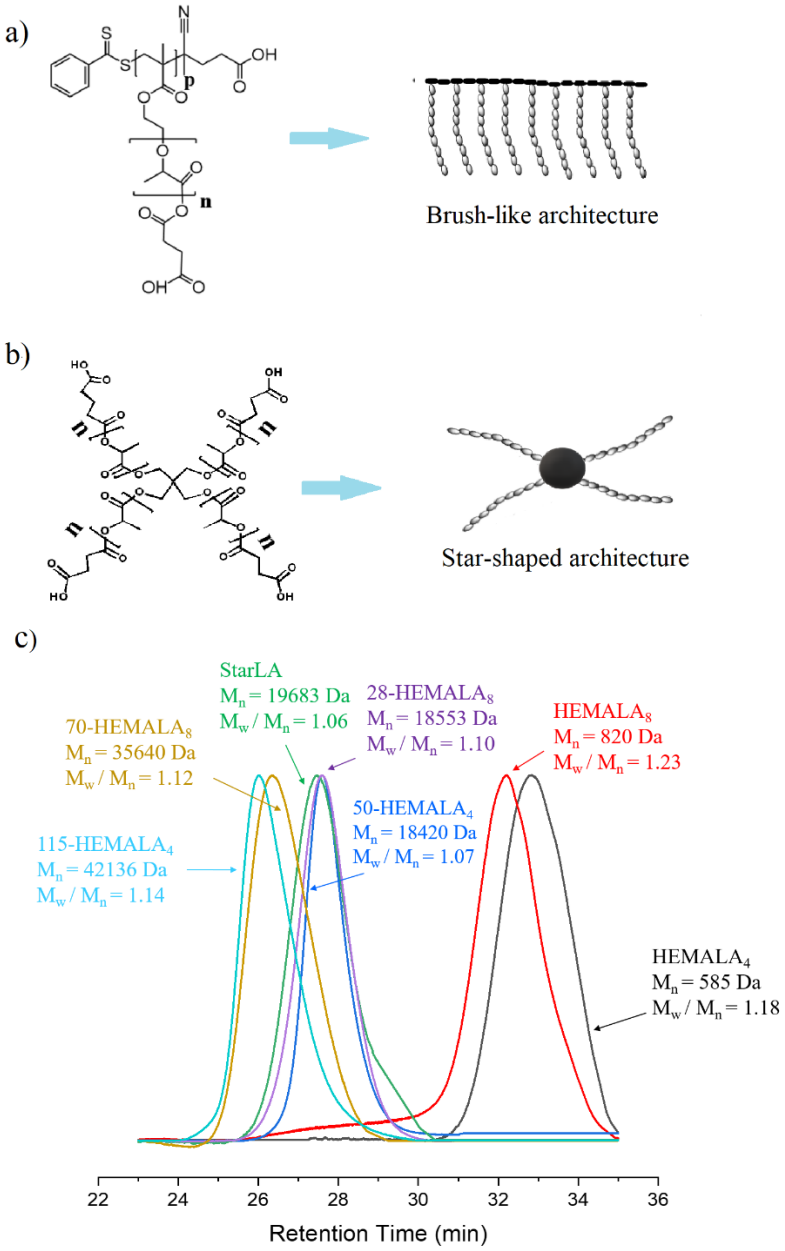

Figure 1: Chemical structure and schematic representation of brush-like (a) and star-shaped (b) structures. (c) Molecular weight distribution of the macromonomers and polymers with different characteristics analysed via Gel Permeation Chromatograph showing the high control over the molecular weight varying the polymer architecture and number and length of the side chains.

In addition, aliquots of the macromonomers were successfully functionalized with succinic anhydride (see **Figure S2** and **Table S1**). This was done in order to provide the macromonomers with a carboxylic end-group able to interact electrostatically with OHC.

Table 1: Targeted degree of polymerization (Targeted DP), Monomer conversion (X), average degree of polymerization (DP), number average molecular weight (Mn) and dispersity (Đ) of the macromonomers and polymers synthesized.

Sample	Targeted DP (-)	X (%)	DP (-)	M_n (Da)	Đ (-)
$HEMALA_4$	4	98.6	4.1	585	1.18
$HEMALA_8$	8	97.7	8.0	820	1.23
50-$HEMALA_4$	50	89.2	44.0	18420	1.07
40-$HEMALA_{4\text{-}COOH}$	40	88.5	37.5	19727[a]	-
115-$HEMALA_4$	115	82.9	118.9	42136	1.14
95-$HEMALA_{4\text{-}COOH}$	95	80.2	93.8	40100 [a]	-
28-$HEMALA_8$	28	95.9	26.9	18553	1.10
25-$HEMALA_{8\text{-}COOH}$	25	99.5	24.9	19267 [a]	-
70-$HEMALA_8$	70	83.7	71.1	35640	1.12
60-$HEMALA_{8\text{-}COOH}$	60	85.5	67.1	42750 [a]	-
50-$HEMALA_4$ (CPA-MeOH)	50	89.3	47.2	23417	1.18
115-$HEMALA_4$ (CPA-MeOH)	115	89.5	130.0	48026	1.26
StarLA	260	82.5	247.0	19683	1.06
$StarLA_{COOH}$	255	82.5	250.0	16900 [a]	-

[a]molecular weight estimated from the ^{1}H-NMR conversion.

Then, the final brush structure shown in **Figure 1a** was achieved *via* solution RAFT polymerization of the aforementioned macromonomers. Polymers with number average molecular weight (Mn) of 20 kg/mol and 50 kg/mol were targeted by defining the proper degree of polymerization (*p*) for each macromonomer. This could be achieved *via* RAFT polymerization by setting to *p* the molar ratio between the macromonomer and the RAFT agent[41]. Hereinafter the brush polymers will be indicated as *p*-$HEMALA_{n\text{-}(COOH)}$. In this way, polymer chains with the same molecular weight but with different side chain lengths and numer of ionizable groups were produced. This enabled to decouple the molecular weight of the polymer from the number of side chains, thus allowing the quantitative evaluation of the effect of a different number of ionizable groups at a given Mn over the OHC renention in the corresponding NPs. High monomer conversions, narrow molecular weight distributions (**Figure 1c**) and average degrees of polymerization close to the targets were obtained for all of the samples, as shown in **Table 1** (see **Figure S3** for the ^{1}H-NMR characterization).

Regarding the star-shaped structure schematically depicted in **Figure 1b**, the polymer was synthesized *via* ROP using pentaerythritol as initiator and LA as monomer. The number of hydroxyl groups on the initiator molecule determines the final number of arms composing the structure of the polymer. Also in this case, the adoption of a controlled polymerization allowed to tune the chain length of every arm based on the molar ratio between the LA and the hydroxyl groups in the intiator. Indeed, the achievement of a good conversion and the desired molecular weight, *i.e* 20 kDa, are confirmed in **Table 1** and **Figure S5**. Moreover, part of the material was successfully functionalized with succinic anhydride through nucleophilic addition in order to add ionizable groups to the structure as shown in **Table 1** and **Figure S6**.

With these polymers, we produced NPs loaded with OHC directly during their formation through the sonication/emulsion and solvent evaporation method as schematically shown in **Figure 2a.**

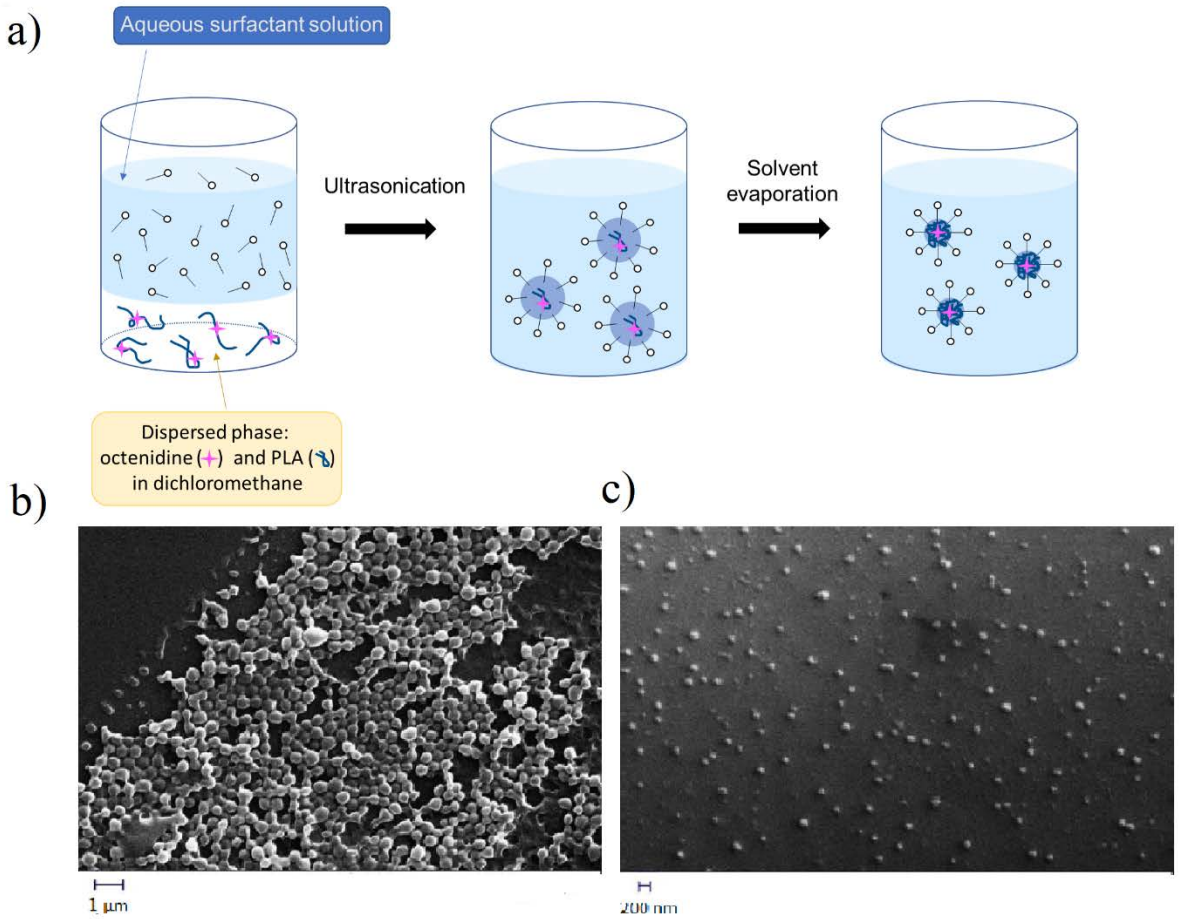

Figure 2: a) Illustration of the process of NP synthesis and OHC encapsulation via sonication/emulsion and solvent evaporation technique. b) SEM micrographs of star-shaped polymer-based NPs (entry 11 in Table S2); c) SEM micrographs of brush-like polymer-based NPs (entry 1 in Table S2).

The applicability of this process to the formulation was guaranteed by the common solubility of the drug and the polymer in dichloromethane. Moreover, the use of a biocompatible stabilizer as TWEEN 80 provided a good stability to the colloidal system, without influencing the particle surface charge since it is a non-ionic surfactant. With this process, we synthesized narrowly dispersed NPs sharing similar size and in particular an average diameter *Dn* in the range 150 - 200 nm as reported in **Table S2**. This NP size makes these colloids suitable for intravenous delivery. For this application, an average NP size between 30 and 300 nm is recommended to avoid rapid renal clearance if the NPs are too small or thrombosis and rapid elimination torugh the liver and the spleen if they are too big [42]. Furthermore, this indicated that the particle size is mainly influenced by the sonication parameters and not by the polymer characteristics. In addition, the different polymer structures do not influence the NP morphology as shown in the SEM micrographs reported in **Figure 2b-c**. Here, spherical and narrowly dispersed NPs with an average size in good agreement with the DLS data for both star-shaped and brush-like polymers can be appreciated. The very narrow size range and spherical morphology allowed us to neglect the effect of the particle size and morphology over the drug release and encapsulation efficiency, relating these parameters uniquely to the polymer features. Finally, the presence of OHC in the colloidal system is confirmed by the ζ-potential of the NPs. Indeed, the functionalized ones present a neutral charge due to the complexation of the ionizable groups in the polymeric chains with the drug. In this case, the colloidal stability is preserved mainly

throught the elastic-steric effect provided by TWEEN 80. On the other hand, the NPs without carboxylic groups show a positive charge related to the ammonium groups of OHC (see **Table S2**).

3.2 Drug encapsulation

The effect of the different polymer characteristics over the behavior of the final formulation as drug carrier was first studied analyzing the OHC encapsulation efficiency, calculated according to **Equation 1**. First, it is worth noticing that for neutral polymers, the encapsulation efficiency is always lower than 30%, and this value is only poorly affected by the molecular weight or polymer architecture, as shown in **Figure 3a-c**. This proves the difficulty in encapsulating charged active principles in non-functionalized polyester NPs exploiting only their entrapment during the NP formation.

A remarkable improvement can be obtained with the addition of functional carboxyl end-groups. Specifically, as shown in **Figure 3a-c**, the presence of ionizable carboxyl end-groups enabled to significantly increase the OHC encapsulation efficiency with respect to their non-functionalized counterparts for all the polymer structures and the molecular weights synthesized. In fact, the ionization of the carboxylic group at phisiologycal pH determines a negative charge in the NPs enabling the electrostatic interaction with the positive charges of OHC. In addition, the encapsulation efficiency can be optimized by varying the polymer microstructure. In fact, the brush-like architecture allows a higher number of end-groups per polymer chain than the star-shaped one and thus a stronger electrostatic interaction that results in a higher capacity to retain the drug during the NP formation. This is confirmed also focusing on the brush structure itself. Precisely, the shorter the oligoester side chain, which means a higher number of negatively charged groups added to the polymeric chain at a given Mn, the higher the amount of drug present in the NPs. This phenomenon is quantified in **Figure 3d**, where the encapsulation efficacy is reported as a function of the moles of carboxyl groups per single NP. We found that the encapsulation efficiency is a linear function of the moles of carboxyl groups in each NP, thus proving that the electrostatic interaction plays a key role in the capacity to encapsulate quaternary ammonium salts as OHC into polymeric biodegradable colloids. This parameter can be conveniently exploited to finely control the encapsulation and consequently the initial burst of the antiseptic from the formulation.

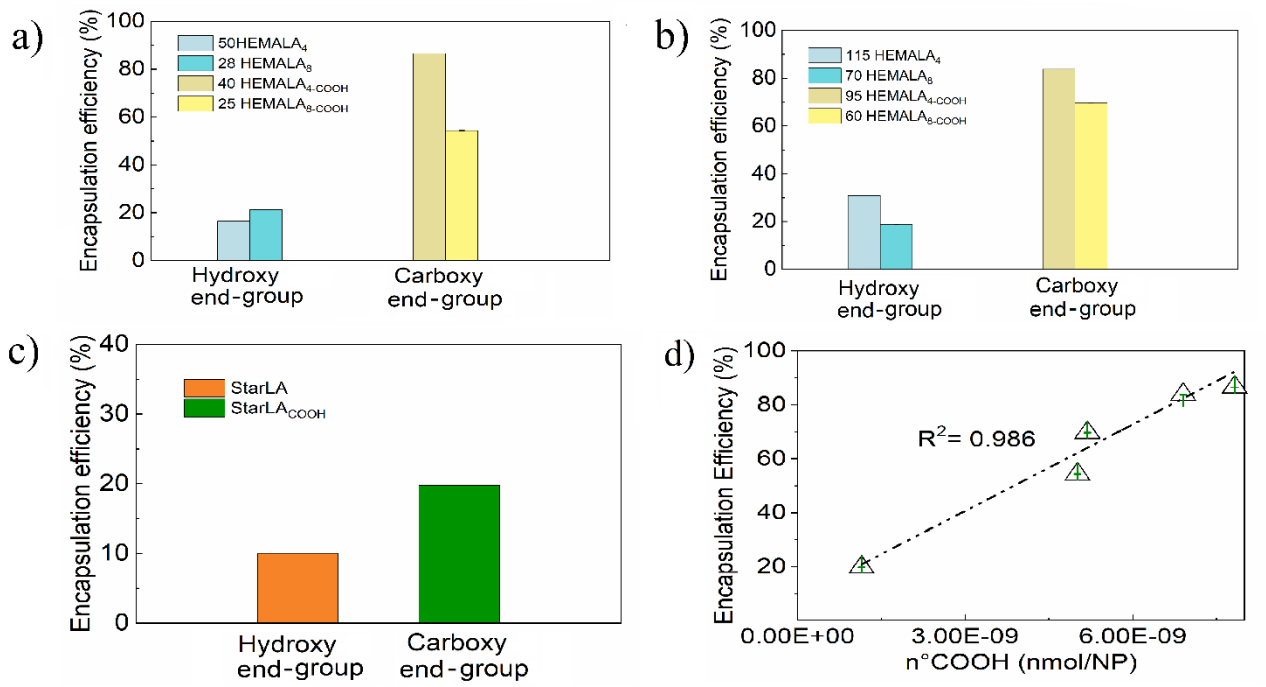

Figure 3: Encapsulation efficiency of: (a) brush- like polymers with Mn = 20 kDa, (b) brush-like polymers with Mn = 50 kDa, (c) star-shaped polymers with Mn = 20 kDa. (d) Trend of encapsulation efficiency varying the moles of carboxyl groups per NP.

3.3 Drug release from NPs

Another aspect that we related to the polymer microstructure and number of functional end-groups is the ability of the produced NPs to mediate the OHC release for a prolonged time. This is pivotal to achieve a long lasting antiseptic action minimizing its inherent toxicity as well as the frequency of administrations. Therefore, we tracked the OHC release from the synthesized NPs for 15 days in order to gather information both on the initial burst and on the long term release of the drug from the particles. First, as shown in **Figure 4a-c**, the NPs composed of non-functionalized polymers led to a significant burst release of OHC, with more than 60% of drug released within the first 2 h. This can be attributed to the poor ability of lipophilic NPs to retain water-soluble drugs like OHC. Of course this limits the application of such NPs in the clinic, as they cannot prevent the side effects related to a massive concentration of OHC. Indeed, regarding non-functionalized polymers, in **Figure 4a-b** we noticed that the NPs composed of polymers with a higher molecular weight released more OHC during the timespan analysed compared to their low molecular weight counterparts. This may be due to the fact that the polymer backbone is terminated with a carboxyl group belonging to the RAFT agent adopted during the synthesis. Therefore, since all the NPs share comparable size and the same concentration, the higher the molecular weight and the lower the number of polymer chains in each NP, with in turn a lower amount of -COOH groups per NP. In order to confirm this hypothesis, NPs composed of brush-like polymers synthesized using the capped RAFT agent CPA-MeOH were produced (**Table 1** and **Table S2**). The comparison in terms of OHC release during the first 24 h for brush-like polymers with carboxy and methyl terminated backbones sharing similar molecular weight

is shown in **Figure S8.** This confirmed that the total absence of an ionizable group in the polymer significantly decreases its capacity to retain the drug.
Therefore, we evaluated the OHC release from NPs composed of functionalized polymers, to verify the relationship between the amount of released OHC after 15 days and the number of carboxyl groups. In this case, the polymer architecture plays a significant role. Indeed, it can be observed that brush-like polymers (**Figure 4a-b**) are able to efficiently retain OHC in the timeframe of the analysis, leading to a sustained release useful to maintain the OHC within a theoretical therapeutic window for more than 15 days. On the other hand, the star-shaped samples (**Figure 4c**), mainly due to the low number of carboxyl groups, were characterized by a significant burst release, comparable with that of the non-functionalized polymers.

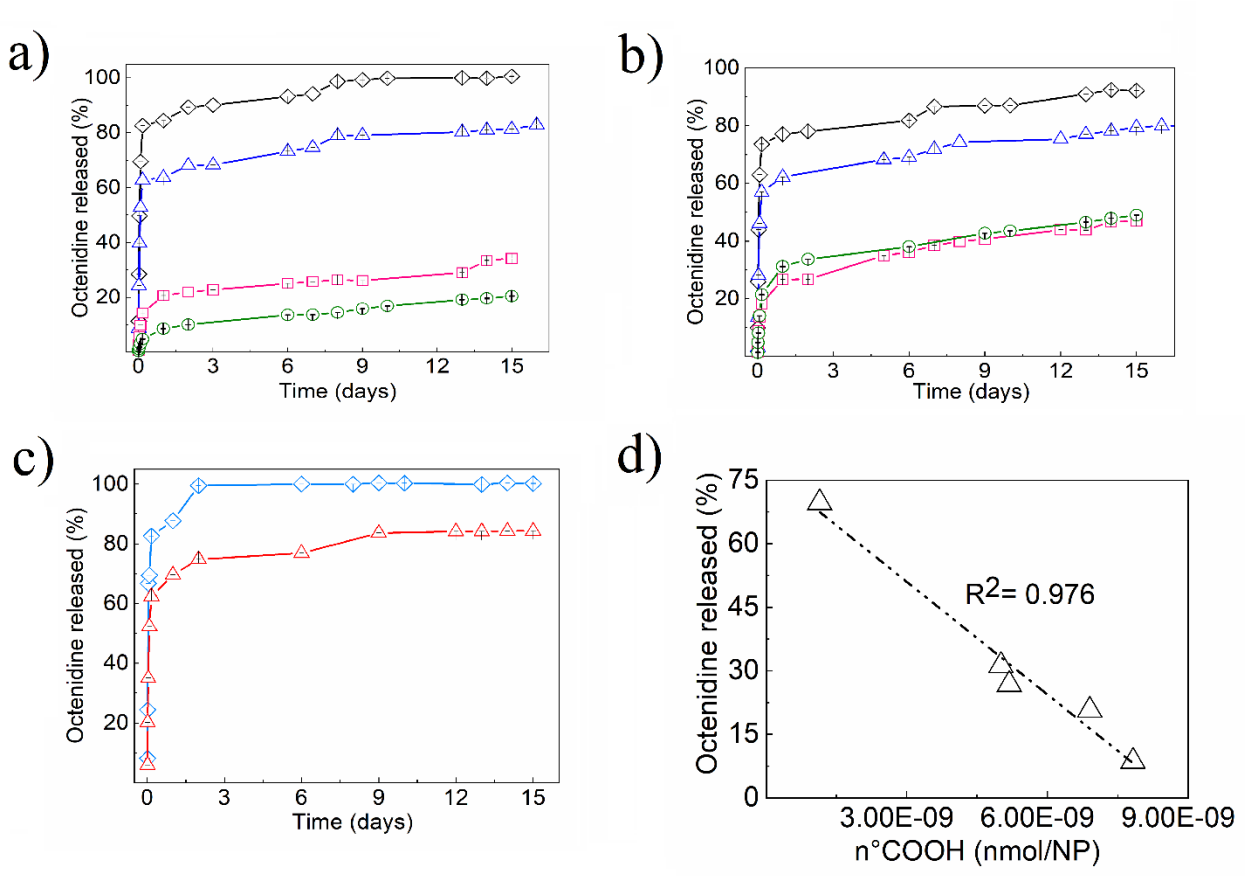

Figure 4: a) OHC release during time for NPs composed of brush-like poly(HEMALA4): 115-HEMALA4 (◊), 50-HEMALA4 (△), 95-HEMALA4-COOH (□), 40-HEMALA4-COOH (○); b) OHC release during time for NPs composed of brush-like poly(HEMALA8): 70-HEMALA8 (◊), 28-HEMALA8 (△), 60-HEMALA8-COOH (□), 25-HEMALA8-COOH (○); c) OHC release during time from NPs composed of star-shaped polymers: StarLA (◊), StarLACOOH (△); d)) Trend of OHC released (%) after 15 days varying the moles of carboxylic groups per NP.

In addition, with the brush-like microstructure we were able to control the number of charged groups present inside the polymer chains and thus in each NP. This is useful to modulate the electrostatic interaction with OHC and in turn its release rate. In fact, as shown in **Figure 4d,** the amount of drug released after 15 days by the formulation is a linear function of the moles of carboxyl groups per NP. To support this experimental evidence we simulated the phase of sustained release with a first-order model and related the kinetic constant k to the moles of –COOH groups per NP. In particular, the amount of released OHC was simulated after the initial burst lasting t_b according to **Equation 3**.

$$Q(t) = 1 - [(1 - Q_b)e^{-k(t-t_b)}] \quad (3)$$

Where $Q(t)$ is the percentage of OHC released at time t, Q_b represents the amount of OHC released by the system at the time t_b corresponding to the initial burst of 24 h and k is the first-order kinetic constant. The comparison between the experimental data and the results from the simulation shown in **Figure 5a** confirms that a first-order model describes satisfyingly well the release of OHC from ionizable NPs. Moreover, we showed in **Figure 5b**, that there is a linear dependence between the first-order kinetic constant *k* and the moles of carboxyl groups per NP, proving that the number of ionizable groups per NP strongly influences the ability of retaining OHC.

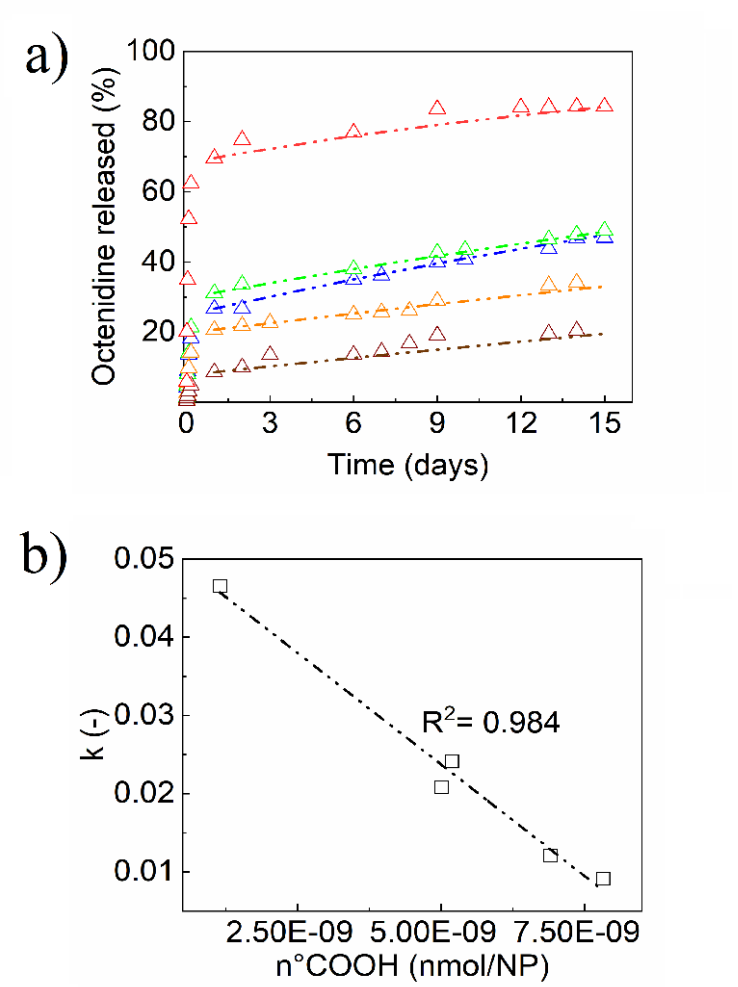

Figure 5: a) Kinetic of Octenidine released over the time for functionalized polymers both measured experimentally (scattered triangles) and predicted by a first-order model (dashed lines) for: 40-HEMALA$_{4\text{-}COOH}$ (brown, R^2= 0.953), 25-HEMALA$_{8\text{-}COOH}$ (green, R^2= 0.997), 60-HEMALA$_{8\text{-}COOH}$ (blue, R^2= 0.992, 95-HEMALA$_{4\text{-}COOH}$ (orange, R^2= 0.931) and STARCOOH (red, R^2= 0.905); b) trend of the first-order kinetic constant (k) over the moles of carboxylic groups per NP.

In addition, for all the NPs analysed, their size (*Dn*) and polydispersity (PdI) were analysed before and after the drug release in order to assess the stability of the systems throughout 15 days. As reported in **Table S2-S3** (Supporting Information), the stability of the colloidal systems was confirmed since no significant changes neither in the size nor in the PdI was measured. Finally, the release of the drug from the polymeric formulation was also further verified through the evaluation of the ζ-potential of the particles before and after the release tests (see **Table S2-S3**). Indeed, after

the release, all the NPs showed lower ζ-potential values than the ones after the synthesis of the formulation, confirming the release of the positively charged OHC.

4 Conclusions

In this work, we studied how the microstructure and chemical functionalization of the polymers composing PLA-based biodegradable NPs enable to control the encapsulation efficiency and prolonged release of the positively charged antiseptic OHC. Two polymer structures, brush-like and star-shaped, with different molecular weights and eventually functionalized with carboxyl end-groups were produced through the combination of ROP and RAFT polymerization and their effect in the formulation was studied. The sonication/emulsion and solvent evaporation method was used to formulate the produced polymers into NPs with comparable size, which allowed to neglect the effect of this parameter in the release of OHC. It was demonstrated that the electrostatic interaction between the polymer and the cationic drug is the dominant driving force that influences both the encapsulation and the release of the active principle. In particular, we observed a linear dependence between the moles of charged groups per NP and the capacity of the formulation to initially retain the drug and provide its sustained release during time. Then, a first-order model describing the drug release from this type of system was proposed and the linear dependence of the kinetic constant from the moles of ionizable groups in the NPs was showed. Finally, it was highlighted the importance of the polymer architecture in order to finely tune the number of ionizable groups in the polymeric chain, thus providing guidelines for adapting the initial burst and the release rate of the formulation to the specific application. The high control we were able to achieve with this polymeric formulation on the encapsulation and release of OHC allows the maintenance of the drug concentration within a tunable therapeutic window, thus paving the way to the safe application of quaternary ammonium salts as antimicrobial agents for *in vivo* therapies.

Supporting Material: Electronic supporting information are available on the publisher website and report the full ^{1}H-NMR characterization of the synthesized polymers, the parameters of all the NPs synthesized, the proof of preserved NP stability and octenidine release after the release test and the release profile of the carboxy-free NPs compared to the not functionalized one.

Conflict of Interests: The authors declare no conflict of interests for this work.

References

1. Salata, O. V (2004) Applications of nanoparticles in biology and medicine. *J. Nanobiotechnology*, **2** (1), 3.
2. Moscatelli, D., and Sponchioni, M. (2017) Bioresorbable polymer nanoparticles in the medical

and pharmaceutical fields, in *Bioresorbable Polymers for Biomedical Applications* (eds.Perale, G., and Hilborn, J.B.T.-B.P. for B.A.), Elsevier, pp. 265–283.

3. Sponchioni, M. (2020) Polymeric nanoparticles for controlled drug delivery, in *Nanomaterials for Theranostics and Tissue Engineering*, Elsevier, pp. 1–28.

4. Bivas-Benita, M., Romeijn, S., Junginger, H.E., and Borchard, G. (2004) PLGA–PEI nanoparticles for gene delivery to pulmonary epithelium. *Eur. J. Pharm. Biopharm.*, **58** (1), 1–6.

5. Panyam, J., and Labhasetwar, V. (2003) Biodegradable nanoparticles for drug and gene delivery to cells and tissue. *Adv. Drug Deliv. Rev.*, **55** (3), 329–347.

6. Ferrari, R., Talamini, L., Violatto, M.B., Giangregorio, P., Sponchioni, M., Morbidelli, M., Salmona, M., Bigini, P., and Moscatelli, D. (2017) Biocompatible Polymer Nanoformulation To Improve the Release and Safety of a Drug Mimic Molecule Detectable via ICP-MS. *Mol. Pharm.*, **14** (1), 124–134.

7. Sponchioni, M., Rodrigues Bassam, P., Moscatelli, D., Arosio, P., and Capasso Palmiero, U. (2019) Biodegradable zwitterionic nanoparticles with tunable UCST-type phase separation under physiological conditions. *Nanoscale*, **11** (35), 16582–16591.

8. Pinto-Alphandary, H., Andremont, A., and Couvreur, P. (2000) Targeted delivery of antibiotics using liposomes and nanoparticles: Research and applications. *Int. J. Antimicrob. Agents*, **13** (3), 155–168.

9. Cheow, W.S., and Hadinoto, K. (2011) Factors affecting drug encapsulation and stability of lipid-polymer hybrid nanoparticles. *Colloids Surfaces B Biointerfaces*, **85** (2), 214–220.

10. Sponchioni, M., Palmiero, U.C., and Moscatelli, D. (2017) HPMA-PEG Surfmers and Their Use in Stabilizing Fully Biodegradable Polymer Nanoparticles. *Macromol. Chem. Phys.*, **218** (23), 1–12.

11. Hans, M.L., and Lowman, A.M. (2002) Biodegradable nanoparticles for drug delivery and targeting. *Curr. Opin. Solid State Mater. Sci.*, **6** (4), 319–327.

12. Kamaly, N., Yameen, B., Wu, J., and Farokhzad, O.C. (2016) Degradable Controlled-Release Polymers and Polymeric Nanoparticles: Mechanisms of Controlling Drug Release. *Chem. Rev.*, **116** (4), 2602–2663.

13. Cingolani, A., Casalini, T., Caimi, S., Klaue, A., Sponchioni, M., Rossi, F., and Perale, G. (2018) A methodologic approach for the selection of bio-resorbable polymers in the development of medical devices: The case of poly(L-lactide-co-ε-caprolactone). *Polymers (Basel).*, **10** (8), Article No. 851.

14. Holland, S.J., Tighe, B.J., and Gould, P.L. (1986) Polymers for biodegradable medical devices. 1. The potential of polyesters as controlled macromolecular release systems. *J. Control. Release*, **4** (3), 155–180.

15. Lassalle, V., and Ferreira, M.L. (2007) PLA Nano- and Microparticles for Drug Delivery: An Overview of the Methods of Preparation. *Macromol. Biosci.*, **7** (6), 767–783.

16. Mohamed, F., and van der Walle, C.F. (2008) Engineering Biodegradable Polyester Particles With Specific Drug Targeting and Drug Release Properties. *J. Pharm. Sci.*, **97** (1), 71–87.

17. Molavi, F., Barzegar-Jalali, M., and Hamishehkar, H. (2020) Polyester based polymeric nano and microparticles for pharmaceutical purposes: A review on formulation approaches. *J.*

Control. Release, **320**, 265–282.

18. Berriós-Torres, S.I., Umscheid, C.A., Bratzler, D.W., Leas, B., Stone, E.C., Kelz, R.R., Reinke, C.E., Morgan, S., Solomkin, J.S., Mazuski, J.E., Dellinger, E.P., Itani, K.M.F., Berbari, E.F., Segreti, J., Parvizi, J., Blanchard, J., Allen, G., Kluytmans, J.A.J.W., Donlan, R., and Schecter, W.P. (2017) Centers for disease control and prevention guideline for the prevention of surgical site infection, 2017. *JAMA Surg.*, **152** (8), 784–791.

19. Deptuła, A., Trejnowska, E., Dubiel, G., Żukowski, M., Misiewska-Kaczur, A., Ozorowski, T., and Hryniewicz, W. (2017) Prevalence of healthcare-associated infections in Polish adult intensive care units: summary data from the ECDC European Point Prevalence Survey of Hospital-associated Infections and Antimicrobial Use in Poland 2012–2014. *J. Hosp. Infect.*, **96** (2), 145–150.

20. Control, E.C. for D.P. and (2008) *ANNUAL EPIDEMIOLOGICAL REPORT ON COMMUNICABLE DISEASES IN EUROPE 2008*.

21. Davies, J. (1996) Origins and evolution of antibiotic resistance. *Microbiologia*, **12** (1), 9–16.

22. Gardete, S., and Tomasz, A. (2014) Mechanisms of vancomycin resistance in Staphylococcus aureus. *J. Clin. Invest.*, **124** (7), 2836–2840.

23. Klevens, R.M., Morrison, M.A., Nadle, J., Petit, S., Gershman, K., Ray, S., Harrison, L.H., Lynfield, R., Dumyati, G., Townes, J.M., Craig, A.S., Zell, E.R., Fosheim, G.E., McDougal, L.K., Carey, R.B., Fridkin, S.K., and Active Bacterial Core surveillance (ABCs) MRSA Investigators, for the (2007) Invasive Methicillin-Resistant Staphylococcus aureus Infections in the United States. *JAMA*, **298** (15), 1763–1771.

24. Lee, J.Y.H., Monk, I.R., Gonçalves da Silva, A., Seemann, T., Chua, K.Y.L., Kearns, A., Hill, R., Woodford, N., Bartels, M.D., Strommenger, B., Laurent, F., Dodémont, M., Deplano, A., Patel, R., Larsen, A.R., Korman, T.M., Stinear, T.P., and Howden, B.P. (2018) Global spread of three multidrug-resistant lineages of Staphylococcus epidermidis. *Nat. Microbiol.*, **3** (10), 1175–1185.

25. Harding, J.L., and Reynolds, M.M. (2014) Combating medical device fouling. *Trends Biotechnol.*, **32** (3), 140–146.

26. Tischer, M., Pradel, G., Ohlsen, K., and Holzgrabe, U. (2012) Quaternary ammonium salts and their antimicrobial potential: Targets or nonspecific interactions? *ChemMedChem*, **7** (1), 22–31.

27. Alvarez-Marin, R., Aires-de-Sousa, M., Nordmann, P., Kieffer, N., and Poirel, L. (2017) Antimicrobial activity of octenidine against multidrug-resistant Gram-negative pathogens. *Eur. J. Clin. Microbiol. Infect. Dis.*, **36** (12), 2379–2383.

28. Zumtobel, M., Assadian, O., Leonhard, M., Stadler, M., and Schneider, B. (2009) The antimicrobial effect of Octenidine-dihydrochloride coated polymer tracheotomy tubes on Staphylococcus aureus and Pseudomonas aeruginosa colonisation. *BMC Microbiol.*, **9** (1), 150.

29. Sedlock, D.M., and Bailey, D.M. (1985) Microbicidal activity of octenidine hydrochloride, a new alkanediylbis[pyridine] germicidal agent. *Antimicrob. Agents Chemother.*, **28** (6), 786 LP – 790.

30. Hübner, N.-O., Siebert, J., and Kramer, A. (2010) Octenidine Dihydrochloride, a Modern Antiseptic for Skin, Mucous Membranes and Wounds. *Skin Pharmacol. Physiol.*, **23** (5), 244–258.

31. Bartoszewicz, M., Rygiel, A., Krzemiński, M., and Przondo-Mordarska, A. (2007) Penetration of a selected antibiotic and antiseptic into a biofilm formed on orthopedic steel implants. *Ortop. Traumatol. Rehabil.*, **9** (3), 310–318.

32. Güzelsağaltici, N., Girgin, S., Gedik, E., Büyükbayram, H., and Baç, B. (2007) Intraperitoneal octenidindihydro-chloride – phenoxyethanol solution to prevent peritoneal adhesion formation in a rat peritonitis model. *Acta Obstet. Gynecol. Scand.*, **86** (4), 395–400.

33. Xu, G., Shen, X., Dai, L., Ran, Q., Ma, P., and Cai, K. (2017) Reduced bacteria adhesion on octenidine loaded mesoporous silica nanoparticles coating on titanium substrates. *Mater. Sci. Eng. C*, **70**, 386–395.

34. Alkhatib, Y., Dewaldt, M., Moritz, S., Nitzsche, R., Kralisch, D., and Fischer, D. (2017) Controlled extended octenidine release from a bacterial nanocellulose/Poloxamer hybrid system. *Eur. J. Pharm. Biopharm.*, **112**, 164–176.

35. Moritz, S., Wiegand, C., Wesarg, F., Hessler, N., Müller, F.A., Kralisch, D., Hipler, U.-C., and Fischer, D. (2014) Active wound dressings based on bacterial nanocellulose as drug delivery system for octenidine. *Int. J. Pharm.*, **471** (1), 45–55.

36. Obermeier, A., Schneider, J., Föhr, P., Wehner, S., Kühn, K.-D., Stemberger, A., Schieker, M., and Burgkart, R. (2015) In vitro evaluation of novel antimicrobial coatings for surgical sutures using octenidine. *BMC Microbiol.*, **15** (1), 186.

37. Michalak, G., Głuszek, K., Piktel, E., Deptuła, P., Puszkarz, I., Niemirowicz, K., and Bucki, R. (2016) Polymeric nanoparticles – a novel solution for delivery of antimicrobial agents. *Med. Stud.*, **1**, 56–62.

38. Baier, G., Cavallaro, A., Friedemann, K., Müller, B., Glasser, G., Vasilev, K., and Landfester, K. (2014) Enzymatic degradation of poly(l-lactide) nanoparticles followed by the release of octenidine and their bactericidal effects. *Nanomedicine Nanotechnology, Biol. Med.*, **10** (1), 131–139.

39. Klaue, A., Maraldi, M., Piviali, C., Moscatelli, D., and Morbidelli, M. (2020) Encapsulation of octenidine hydrochloride into bioresorbable polyesters for extended antimicrobial activity. *Eur. Polym. J.*, **138** (September), 109987.

40. Sponchioni, M., Capasso Palmiero, U., Manfredini, N., and Moscatelli, D. (2019) RAFT copolymerization of oppositely charged monomers and its use to tailor the composition of nonfouling polyampholytes with an UCST behaviour. *React. Chem. Eng.*, **4** (2), 436–446.

41. Capasso Palmiero, U., Sponchioni, M., Manfredini, N., Maraldi, M., and Moscatelli, D. (2018) Strategies to combine ROP with ATRP or RAFT polymerization for the synthesis of biodegradable polymeric nanoparticles for biomedical applications. *Polym. Chem.*, **9** (30).

42. Ferrari, R., Sponchioni, M., Morbidelli, M., and Moscatelli, D. (2018) Polymer nanoparticles for the intravenous delivery of anticancer drugs: the checkpoints on the road from the synthesis to clinical translation. *Nanoscale*, **10** (48), 22701–22719.